

# UC San Diego

## UC San Diego Previously Published Works

### Title

Sub-Seasonal Forcing Drives Year-To-Year Variations of Southern Ocean Primary Productivity

### Permalink

<https://escholarship.org/uc/item/0d11c7fz>

### Journal

Global Biogeochemical Cycles, 36(7)

### ISSN

0886-6236

### Authors

Prend, Channing J  
Keerthi, MG  
Lévy, Marina  
et al.

### Publication Date

2022-07-01

### DOI

10.1029/2022gb007329

Peer reviewed

# Global Biogeochemical Cycles®





## RESEARCH ARTICLE

10.1029/2022GB007329

### Special Section:

Southern Ocean and Climate: Biogeochemical and Physical Fluxes and Processes

## Sub-Seasonal Forcing Drives Year-To-Year Variations of Southern Ocean Primary Productivity

Channing J. Prend<sup>1</sup> , M. G. Keerthi<sup>2</sup>, Marina Lévy<sup>2</sup>, Olivier Aumont<sup>2</sup> , Sarah T. Gille<sup>1</sup> , and Lynne D. Talley<sup>1</sup> 

<sup>1</sup>Scripps Institution of Oceanography, University of California San Diego, La Jolla, CA, USA, <sup>2</sup>LOCEAN-IPSL, CNRS, Sorbonne Université, Paris, France

### Key Points:

- Year-to-year variations of annual mean chlorophyll in the Southern Ocean are weakly correlated with the Southern Annular Mode
- Non-seasonal chlorophyll fluctuations are driven by intermittent sub-seasonal events, which dominate the changes in the annual mean
- The spatial autocorrelation for the chlorophyll seasonal cycle is much larger than for variations in the annual mean chlorophyll

### Supporting Information:

Supporting Information may be found in the online version of this article.

### Correspondence to:

C. J. Prend,  
[cprend@ucsd.edu](mailto:cprend@ucsd.edu)

### Citation:

Prend, C. J., Keerthi, M. G., Lévy, M., Aumont, O., Gille, S. T., & Talley, L. D. (2022). Sub-seasonal forcing drives year-to-year variations of Southern Ocean primary productivity. *Global Biogeochemical Cycles*, 36, e2022GB007329. <https://doi.org/10.1029/2022GB007329>

Received 21 JAN 2022

Accepted 23 JUN 2022

**Abstract** Primary productivity in the Southern Ocean plays a key role in global biogeochemical cycles. While much focus has been placed on phytoplankton production seasonality, non-seasonal fluctuations exceed the amplitude of the seasonal cycle across large swaths of the Antarctic Circumpolar Current. This non-seasonal variability comprises a broad range of timescales from sub-seasonal (<3 months) to multi-annual (>1 year), all of which can project onto the annual mean value. However, year-to-year variations of surface chlorophyll (SChl), a proxy for phytoplankton biomass, are typically attributed to ocean circulation changes associated with the Southern Annular Mode (SAM), which implicitly assumes that sub-seasonal variability averages to near-zero over long timescales. Here, we test this assumption by applying a timeseries decomposition method to satellite-derived SChl in order to separate the low-frequency and high-frequency contributions to the non-seasonal variability. We find that throughout most of the Southern Ocean, year-to-year SChl variations are dominated by the sub-seasonal component, which is not strongly correlated with the SAM. The multi-annual component, while correlated with the SAM, only accounts for about 10% of the total SChl variance. This suggests that changes in annual mean SChl are related to intermittent forcing at small scales, rather than low-frequency climate variability, and thus do not remain correlated over large regions.

**Plain Language Summary** Microalgae called phytoplankton are the foundation of marine food webs and play a large role in the carbon cycle. Therefore, understanding the mechanisms that drive phytoplankton variability is of critical importance to marine ecosystems and global climate. Phytoplankton growth is known to exhibit a strong seasonal cycle. In addition to this, phytoplankton biomass also varies between years. This variability is often linked to multi-year climate oscillations like El Niño. On short timescales, phytoplankton are also influenced by processes such as storms and eddies, which alter the supply of nutrients and light that they need to grow. In this study, we use satellite measurements to untangle the different timescales of phytoplankton variability in the Southern Ocean, which surrounds Antarctica. We find that year-to-year fluctuations in phytoplankton biomass are driven by intermittent events associated with storms and eddies, rather than multi-year climate oscillations. Therefore, processes occurring at small scales must be considered in order to understand long-term phytoplankton variability and trends related to climate change.

## 1. Introduction

The Southern Ocean is a high-nutrient low-chlorophyll environment where phytoplankton growth is limited primarily by iron and light (de Baar et al., 1995; Mitchell et al., 1991). Physical processes in the ocean impact these controls, subsequently affecting the distribution of phytoplankton across a wide range of spatial and temporal scales (Ardyna et al., 2017; Lévy et al., 2012; Li et al., 2021; Rohr et al., 2017; Rousseaux & Gregg, 2014). Indeed, phytoplankton biomass, inferred from satellite-derived surface chlorophyll (SChl), exhibits variability from sub-seasonal (<3 months) to multi-annual (>1 year) timescales (Arrigo et al., 2008; Frenger et al., 2018; Keerthi et al., 2020; Thomalla et al., 2011). Untangling these disparate scales is necessary to develop a quantitative model of spatiotemporal chlorophyll variability and identify long-term trends associated with climate change, which are currently eclipsed by natural year-to-year variations in most regions globally (Behrenfeld et al., 2006; Gregg & Rousseaux, 2019; Henson et al., 2010; Martinez et al., 2009).

In the Southern Ocean, changes in annual mean SChl have been linked to the Southern Annular Mode (SAM), the leading mode of atmospheric variability in the Southern Hemisphere (Thompson & Wallace, 2000). SAM influences the ocean circulation and stratification in the region, which in turn impacts primary productivity by

modulating nutrient and light availability (Boyd et al., 2008; Lovenduski & Gruber, 2005; Sallée et al., 2010). For example, Lovenduski and Gruber (2005) regressed non-seasonal satellite chlorophyll anomalies onto the SAM index; their results suggest that SChl is positively correlated with the SAM south of the Polar Front (PF) due to increased iron supply by anomalous upwelling, and negatively correlated with the SAM north of the PF due to stronger light limitation stemming from deeper mixed layers.

While this type of analysis has helped discern mechanisms of non-seasonal SChl variability (i.e., the variability that remains after removing the seasonal cycle), there are limitations to this approach. First, using the SAM index as a measure of climate variability neglects significant regional differences in Southern Ocean winds, air-sea heat fluxes, mixed-layer depth (MLD), and the MLD response to forcing (Keppler & Landschützer, 2019; Rintoul, 2018; Sallée et al., 2010; Tamsitt et al., 2015). Second, relating non-seasonal SChl variations to low-frequency climate modes presumes that high-frequency variability averages to near-zero on annual and longer timescales. However, many studies have documented large amplitude sub-seasonal SChl fluctuations throughout the global ocean (Bonhomme et al., 2007; Resplandy et al., 2009), and particularly in the Southern Ocean (Fauchereau et al., 2011; Joubert et al., 2014; Little et al., 2018). Therefore, here we investigate whether these transient processes imprint on the annual mean and year-to-year variations of Southern Ocean primary production (Little et al., 2018).

Following Keerthi et al. (2020), we decompose satellite-derived SChl into three frequency ranges: sub-seasonal (~0.5–3 months), seasonal (~3–12 months), and multi-annual (>12 months). We show that there are distinct regional differences in the dominant timescale of SChl variability. For example, the seasonal cycle accounts for most of the variance in the subtropics, while non-seasonal variability dominates in most other parts of the Southern Ocean. This non-seasonal SChl variability primarily reflects sub-seasonal fluctuations, which occur over small spatial scales (~50–150 km) and are not strongly correlated with the SAM. The importance of high-frequency events is related, in part, to the non-Gaussianity of chlorophyll. The multi-annual component of SChl, by contrast, is correlated with the SAM, but only explains about 10% of the total SChl variance across most of the Antarctic Circumpolar Current (ACC). This suggests that year-to-year variations in annual mean SChl are related to intermittency resulting from localized forcing such as storms and eddies, rather than low-frequency climate modes (Lévy et al., 2014). Consequently, the spatial scales associated with consistent variations in the annual mean are small (~100–300 km), which implies that SChl should not be averaged over large regions to investigate year-to-year changes.

Complementary to satellite ocean color data, recent advances in autonomous observing platforms have dramatically increased the number of subsurface biogeochemical measurements in the Southern Ocean (Johnson et al., 2017; Talley et al., 2019). Fluorescence measurements from autonomous floats have shown good agreement with satellite-derived SChl products, and provide data under clouds and during polar night (Haëntjens et al., 2017). However, given the complex vertical structure of phytoplankton biomass in the Southern Ocean (Carranza et al., 2018; Uchida et al., 2019), fluctuations in SChl do not necessarily reflect changes in the vertically integrated chlorophyll column inventory ( $\text{Chl}_{\text{tot}}$ ). Therefore, we also apply the same timeseries decomposition as we used for the satellite data to float SChl and  $\text{Chl}_{\text{tot}}$  to show that strong sub-seasonal variability in SChl is representative of the integrated signal. These results highlight the importance of small-scale processes in determining the annual mean SChl and its variability.

## 2. Data and Methods

### 2.1. Observational Datasets

In this study, we use a merged SChl data product from the European Space Agency Ocean Color Climate Change Initiative (ESA OC-CCI) that combines data from multiple ocean color satellites (Sathyendranath et al., 2017) including Moderate Resolution Imaging Spectroradiometer, Sea-Viewing Wide Field-of-View Sensor, MEdium Resolution Imaging Spectrometer and Visible Infrared Imaging Radiometer Suite. We use the Level 3 Mapped  $25 \times 25$  km version at 8-day temporal resolution, which spans 20 years from January 1999 to December 2018 and is publicly available (<http://www.oceancolour.org/>). This merged data product captures a longer time period than any individual satellite, and thus is well-suited for investigations of year-to-year variability. However, as with all ocean color products, there are many data gaps in the Southern Ocean due to cloudiness, ice cover and low sun angles (Arrigo et al., 2008). Locations with less than 50% data coverage over the full record are masked out in this

analysis, although we note that most of the missing data are from austral winter when SChl levels are near-zero due to light limitation.

To evaluate the relationship between temporal variability in SChl and  $\text{Chl}_{\text{tot}}$ , we also use in situ data from autonomous biogeochemical floats deployed by the Southern Ocean and Climate Field Studies with Innovative Tools (SOCLIM) project. SOCLIM floats measure temperature, salinity, pressure, dissolved oxygen, nitrate, fluorescence, backscatter, and photosynthetically available radiation (Pellichero et al., 2020). Here, we analyze quality-controlled data from three SOCLIM floats (float IDs: 6902735, 6902736, 6902737) that sampled in the Kerguelen Plateau region for three years, from September 2016 to September 2019 (<http://soclim.com/>). These floats were selected since they are higher resolution in time and depth than the standard biogeochemical Argo float (10-day cycle time and 5 m resolution in the upper ocean). Data processing is described by Johnson et al. (2017); the raw fluorometer data are transformed to engineering units using the manufacturer calibration coefficients, the dark counts are adjusted using a gain correction, and the profiles are also corrected for nonphotochemical quenching following Xing et al. (2017). SOCLIM floats sampled unevenly in the vertical with roughly 1 m resolution in the upper ocean, and all profiles are linearly interpolated onto a regular depth axis with 5 m resolution. SChl is taken to be the average chlorophyll over the top 20 m, which is approximately the first optical depth (Morel, 1988). While  $\text{Chl}_{\text{tot}}$  is calculated as the vertical integral over the top 200 m of the water column (Grenier et al., 2015; von Berg et al., 2020), results are not sensitive to the precise integration depth. Floats also sampled unevenly in time, with profiles taken daily, every 2 days, and every 4 days at different points during the float lifetime. Here, we take 8-day means of the float data to match the temporal resolution of the satellite SChl product.

Wind data from the Cross-Calibrated Multi Platform (CCMP) product are used to examine some of the forcings that drive SChl variability. CCMP combines wind data from several satellite scatterometers, moored buoys, and a reanalysis product (Atlas et al., 2011). CCMP winds have been shown to be more reliable at high frequencies than any single scatterometer, and have higher correlations with MLD than other wind products (Atlas et al., 2011; Carranza & Gille, 2015). The merged wind product is available on the same  $25 \times 25$  km horizontal grid as the SChl data from ESA OC-CCI. Here, we take 8-day means of the daily winds from 1999 to 2018 (i.e., the ESA OC-CCI period) to correspond directly with the ocean color data. The daily Antarctic Oscillation index (i.e., SAM index) from the NOAA/NCEP Climate Prediction Center from 1999 to 2018 (<http://www.cpc.ncep.noaa.gov/>) was also averaged into 8-day periods to calculate correlations of different fields with the SAM.

## 2.2. Decomposition Method

Here, we decompose SChl timeseries at each grid point into three frequency bands following the method in Keerthi et al. (2020), which is based on the Census X11 iterative algorithm (Vantrepotte & Mélin, 2009). This decomposition uses a series of filters to separate the full SChl signal ( $X_t$ ) into multi-annual ( $T_t$ ), seasonal ( $S_t$ ), and sub-seasonal ( $I_t$ ) components such that  $X_t = T_t + S_t + I_t$ . The multi-annual component,  $T_t$ , is determined by a centered annual running mean and a Henderson filter of weight representing one year, also applied iteratively. The seasonal component,  $S_t$ , captures variability with a period of  $\sim 3$ –12 months and is isolated by taking multiple weighted running means over three consecutive timesteps and then applying an 88-day (i.e., approximately 3 months given the temporal resolution of the data) low-pass filter, iteratively. To account for year-to-year variations in the seasonal cycle, this decomposition method does not assume an annually repeating  $S_t$ . The sub-seasonal component,  $I_t$ , is found by applying a bandpass filter of 8–88 days. Finally, the residual is attributed to the sub-seasonal component, such that the timeseries is exactly decomposed into the sum of the three components. Note that this method does not have sharp frequency cut-offs in order to allow for variations in the dominant period of the seasonal cycle and multiple harmonics in  $S_t$ . Further details of the decomposition method are provided in Keerthi et al. (2020). Figure 2 illustrates the timeseries decomposition at three grid points whose locations are marked in Figure 1.

The total SChl variance is partitioned into the sum of the variance in the multi-annual, seasonal, and sub-seasonal components, as well as the covariances between the terms:  $\text{var}(X_t) = \text{var}(T_t) + \text{var}(S_t) + \text{var}(I_t) + 2\text{cov}(S_t, T_t, I_t)$ . The covariance terms are small (explaining only a few percent of the total variance), so examining the individual variances of  $T_t$ ,  $S_t$ , and  $I_t$  directly quantifies the contribution of each frequency band to the total SChl variance (Figure 3). We also estimate the spatial scales associated with each component of SChl variability by cross-correlating  $T_t$ ,  $S_t$ , and  $I_t$  at a given grid cell with the corresponding components at all other grid cells (Figure

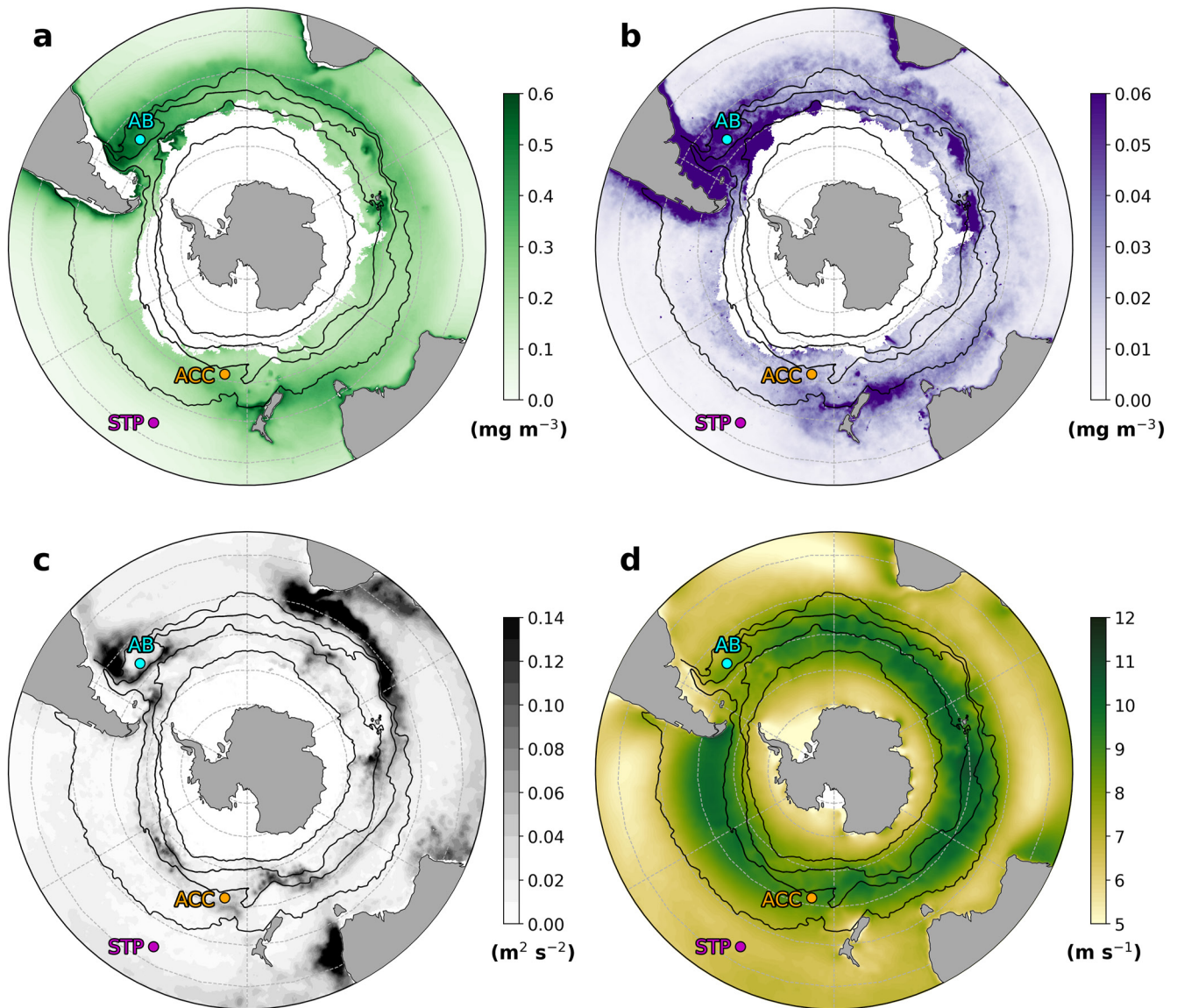


**Figure 1.** (a) 1999–2018 annual mean surface chlorophyll ( $\text{mg}/\text{m}^3$ ) and (b) standard deviation of the annual mean ( $\text{mg}/\text{m}^3$ ) from the European Space Agency Ocean Color Climate Change Initiative merged ocean color product. (c) 1979–2015 mean eddy kinetic energy ( $\text{m}^2/\text{s}^2$ ) from surface drifters (Laurindo et al., 2017) (d) 1999–2018 summer mean wind speed ( $\text{m}/\text{s}$ ) from the Cross-Calibrated Multi Platform merged data product. Colored points in all panels mark the stations whose timeseries are plotted in Figure 2: Subtropical Pacific (magenta), Antarctic Circumpolar Current (ACC) (orange), and Argentine Basin (cyan). Black lines in all panels mark the mean position of the ACC fronts from Kim and Orsi (2014), which are from north to south: Subtropical front, Subantarctic front, Polar front, and Sea Ice Edge.

S1 in Supporting Information S1). From the number of cells where the correlation coefficient exceeds a threshold of 0.8, we then compute the area over which each signal remains consistent and take the length scale to be  $\sqrt{\text{Area}}$ . This threshold value was chosen following Keerthi et al. (2020), although the length scales are similar for a range of threshold values from 0.5 to 0.9 (Figure S2 in Supporting Information S1): namely, 200–400 km, 500–600 km, 50–150 km for the multi-annual, seasonal, and sub-seasonal components, respectively.

### 2.3. Synthetic Data

In order to probe the statistical nature of the results, we also produced two synthetic timeseries with different probability distributions. Both artificial variables have red spectra, which are common for geophysical quantities,

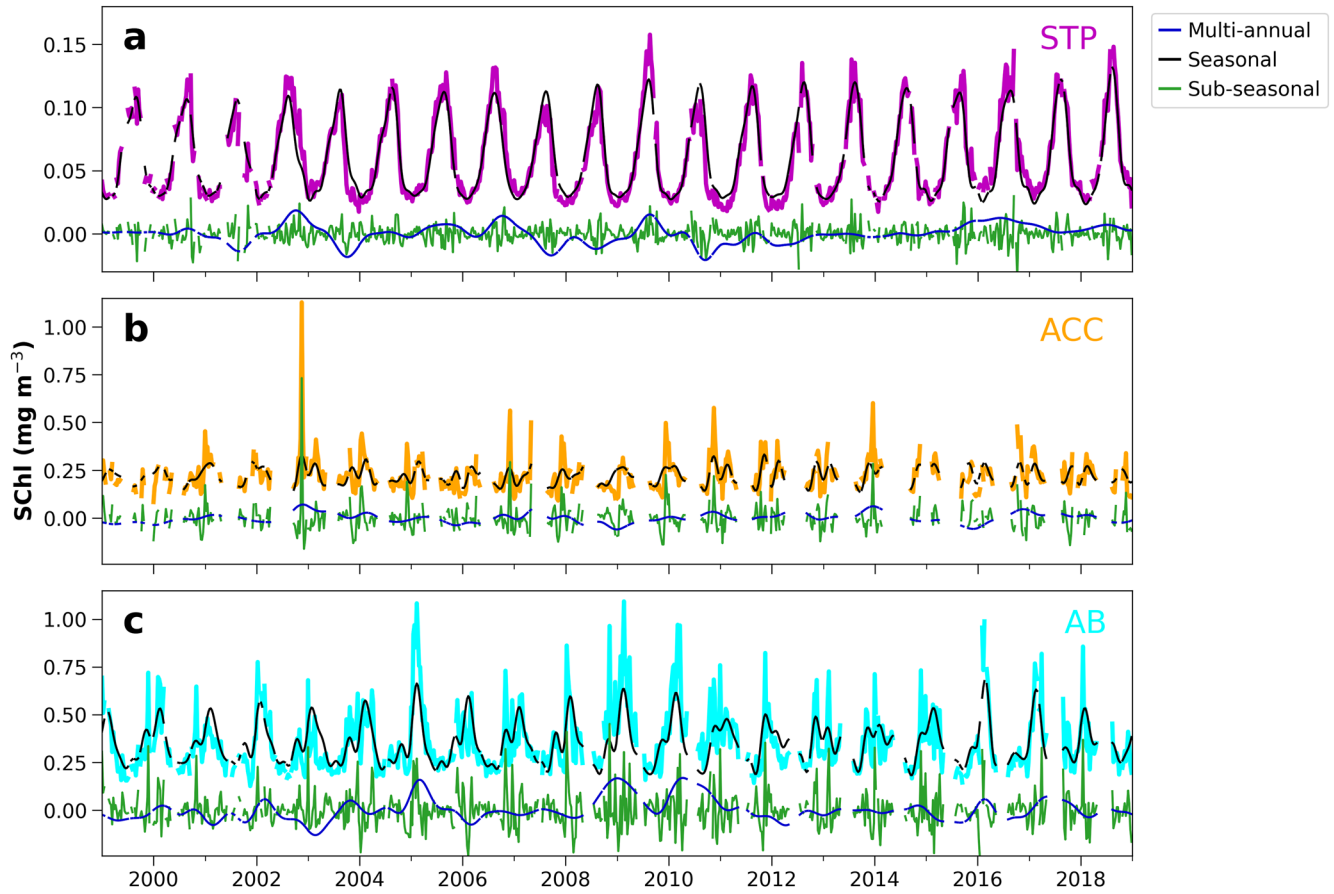


**Figure 2.** Satellite-derived surface chlorophyll timeseries decomposition for three stations marked in Figure 1: (a) Subtropical Pacific (34°S, 152°W), (b) Antarctic Circumpolar Current (52°S, 170°W), and (c) Argentine Basin (46°S, 45°W). The full signal ( $X$ ) is plotted in (a) magenta, (b) orange, and (c) cyan. In all panels the multi-annual component ( $T$ ) is blue, the seasonal component ( $S$ ) is black, and the sub-seasonal component ( $I$ ) is green.

weighted toward low frequencies without a preferred period (Maraun et al., 2007; Schulte et al., 2015; Torrence & Compo, 1998). We generated red noise using an auto-regressive process with a lag-1 autocorrelation coefficient of 0.85, following Allen and Smith (1996). The first artificial variable is zero-mean with a Gaussian distribution (Figure 5a), which is representative of many normally distributed oceanic tracers. SChl, however, has been

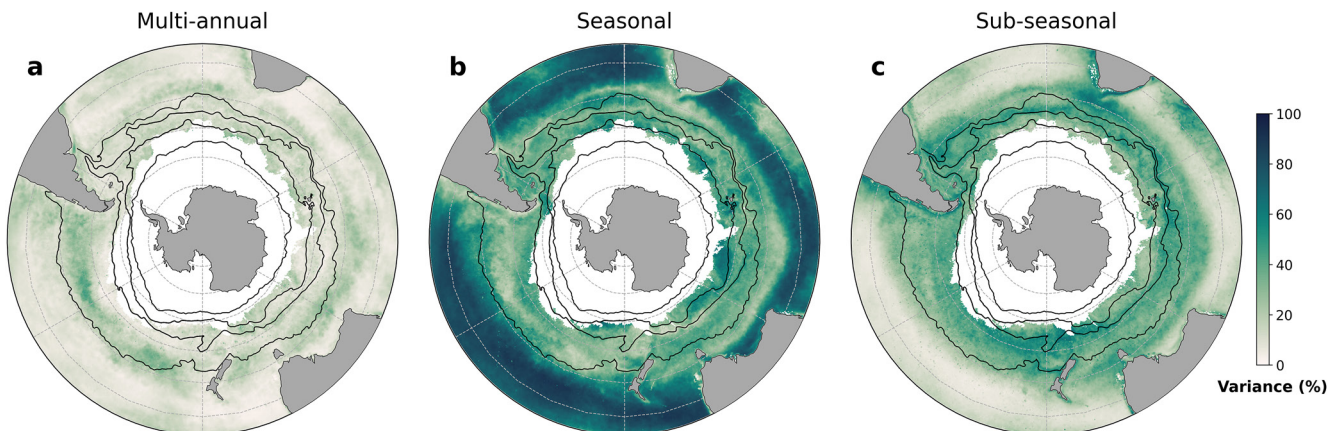


**Figure 3.** Percentage of the total satellite-derived surface chlorophyll (SChl) variance explained by the (a) multi-annual, (b) seasonal, and (c) sub-seasonal components of the SChl decomposition.

observed to follow a log-normal distribution; this is presumably because bio-optical properties in the ocean can be represented as the product of light attenuation coefficients, which would imply that SChl obeys the law of proportionate effect (Campbell, 1995). Therefore, our second artificial variable is taken to be the exponential of the first (Figure 5b), meaning that it is positive-valued and log-normally distributed, like SChl. We then apply the same decomposition method to the synthetic timeseries (Figure S3 in Supporting Information S1), although the three components simply represent high, mid, and low frequency bands since the timesteps are essentially arbitrary (i.e., the red noise cannot be interpreted as having sub-seasonal, seasonal, and multi-annual components). Comparing the results for the two synthetic variables allows us to assess the extent to which the importance of sub-seasonal events to the total SChl variance stems from the log-normality of chlorophyll.

### 3. Results

#### 3.1. Satellite Analysis

Southern Ocean primary production is heterogeneous in space and time. Still, distinct bloom phenology regimes have been identified from satellite SChl, as well as large-scale patterns in the mean (Ardyna et al., 2017; Sallée et al., 2015; Thomalla et al., 2011). Namely, higher annual mean SChl (Figure 1a) is observed in boundary current regions, near fronts, and downstream of islands or topographic features in the path of the ACC (Meredith et al., 2003; Prend et al., 2019; Rosso et al., 2016; Sokolov & Rintoul, 2007). These patterns are related to heterogeneities in iron sources and the pathways that supply iron to the euphotic zone (Graham et al., 2015; Lancelot et al., 2009; Tagliabue et al., 2012). There is also significant spatial variability in the standard deviation of the annual mean (Figure 1b), which somewhat mirrors the structure in the annual mean itself (Figure S4 in Supporting Information S1). Year-to-year variations of SChl are larger within the ACC and in energetic boundary currents with high EKE (Figure 1c). The subtropics (north of the Subtropical front), by contrast, have low SChl values and less variability between years, which coincides with weaker eddy activity and winds (Figure 1d).

Temporal SChl variability also demonstrates major regional differences, which is illustrated by the timeseries in Figure 2. In the subtropics (Figure 2a), SChl resembles a sinusoidal seasonal cycle with little change in amplitude between years, whereas in the open ACC (Figure 2b), SChl fluctuations occurring on weekly timescales greatly exceed the amplitude of the seasonal cycle. Finally, in boundary current regions such as the Brazil-Malvinas confluence (Figure 2c), the seasonal cycle is more prominent than in the open ACC (Figure 2b) but is punctuated by sub-seasonal pulses that significantly increase the magnitude of the annual maximum. These regional patterns in the dominant timescale of SChl variability lead to a fundamentally different interpretation of the annual mean SChl value itself. For example, in the subtropics, where SChl is driven by seasonal variability, annual mean SChl reflects the integrated seasonal bloom. In contrast, in the open ACC, where sub-seasonal variability dominates, annual mean SChl is manifested through the sum of transient bursts that take place throughout spring and summer.

While the details of the timeseries plotted in Figure 2 are unique, we demonstrate that these stations are representative of larger regional regimes by showing maps of the percentage of total SChl variance explained by each frequency range (Figure 3). North of the Subtropical front, the seasonal component explains >70% of the total variance (Figure 3b), consistent with the timeseries in Figure 2a. Moving southward into the ACC, sub-seasonal variability is significantly stronger (Figure 3c), exceeding even the variance explained by the seasonal cycle in many locations, such as the station shown in Figure 2b. This is consistent with Thomalla et al. (2011), who showed the greatest seasonal cycle reproducibility in the subtropics. Across the entire Southern Ocean, the multi-annual component is weak except in a narrow band spanning the Subantarctic Mode Water formation sites in the Pacific, where the deepest winter mixed layers in the entire Southern Ocean are found (Hanawa & Talley, 2001). The comparatively large share of SChl variance explained by the multi-annual component in the mode water formation region may be due to the substantial variations in maximum winter MLD observed there, which have been linked to the SAM (Meijers et al., 2019) and could influence nutrient supply to the euphotic zone.

Non-seasonal SChl variability in the Southern Ocean is dominated by high-frequency rather than low-frequency fluctuations (Figure 3). Averaged across the entire ACC, sub-seasonal variations constitute 47% of the total SChl variance, and 81% of the non-seasonal SChl variance. This helps explain the relatively modest correlations between non-seasonal chlorophyll anomalies and the SAM index (Lovenduski & Gruber, 2005). To further explore this, Figure 4 shows the correlation coefficients between the SAM index and each individual component of the SChl decomposition. The seasonal and sub-seasonal components of SChl are not strongly correlated with

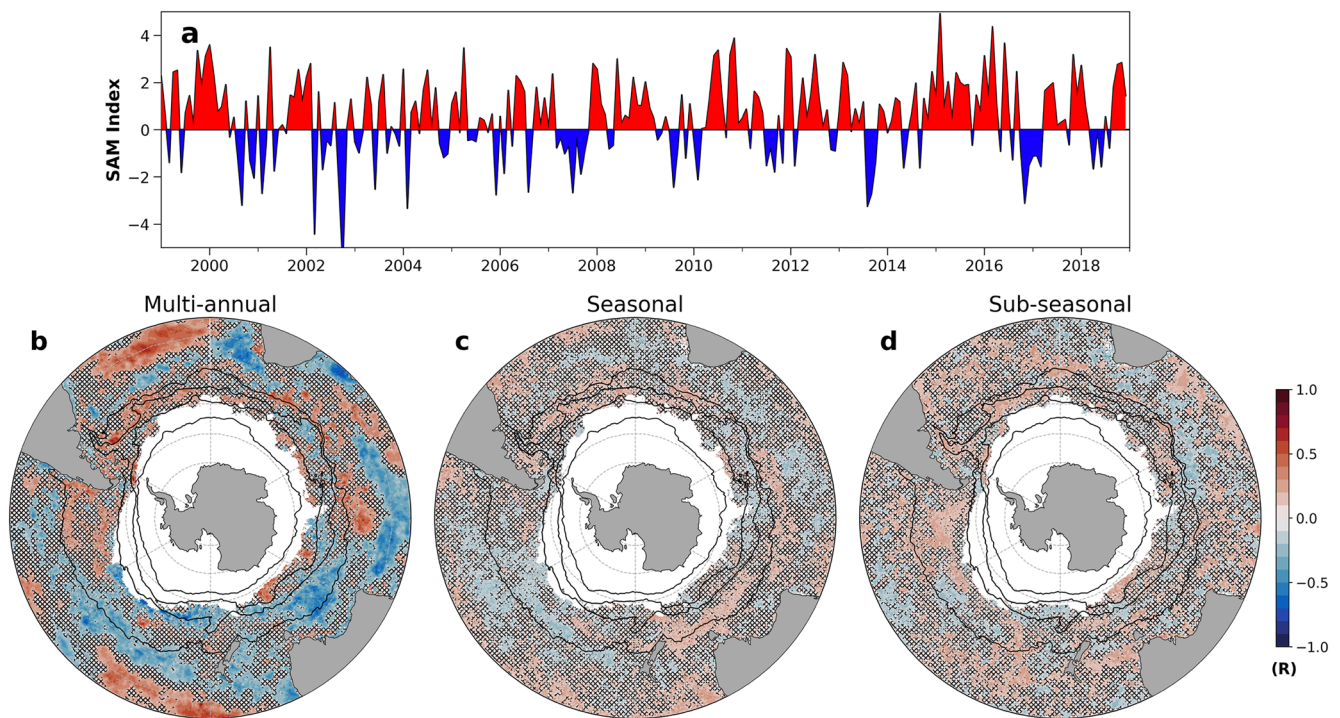


**Figure 4.** (a) 1999–2018 monthly Southern Annular Mode (SAM) index from NOAA/NCEP Climate Prediction Center (bd) Correlation coefficient between the 8-day averages of the daily SAM index (to match the temporal resolution of the satellite satellite-derived surface chlorophyll (SChl) data) and the (b) multi-annual, (c) seasonal, and (d) sub-seasonal components of the SChl decomposition. In all panels, cross-hatching indicates where the correlations are not significant at the 95% level.

the SAM (Figures 4c and 4d). The multi-annual component, while much more highly correlated with the SAM (Figure 4b), only accounts for about 10% of the total SChl variance (Figure 3a). The broad zonal pattern in Figure 4b is consistent with results from Lovenduski and Gruber (2005). However, it is difficult to extract a relationship between satellite SChl and the SAM because the low-frequency SChl variability associated with SAM forcing is overwhelmed by the much larger SChl fluctuations occurring at high frequencies.

### 3.2. Synthetic Data Analysis

The large contribution of high frequencies to the total SChl variance could result from the non-Gaussianity of chlorophyll, since log-normally distributed variables (such as SChl) are known to be heavy tailed (Campbell, 1995). Therefore, synthetic timeseries (Figure 5) with varied probability distributions were used to assess this. Figure S3 in Supporting Information S1 gives the decomposition of the Gaussian and log-normal red noise, and the insets in Figure 5 show the percent variance explained by high, mid, and low frequency bands. The zero-mean, Gaussian red noise has its variance evenly divided between the three components of the decomposition (inset in Figure 5a), whereas the positive-valued, log-normal red noise has a greater portion of its variance, 46%, explained by the high-frequency component (inset in Figure 5b). The sensitivity of these results to the details of the noise formulation have not been explored fully. Our intent is simply to demonstrate that the large magnitude of sub-seasonal SChl variability seen in the satellite data is connected, in part, to its probability distribution, which lends more weight to extreme events due to its heavy tail. However, the partitioning of variance from the satellite SChl data does not appear to result solely from the log-normality of chlorophyll, since the same decomposition method applied to log (SChl) also indicates a disproportionate importance of sub-seasonal variability (Figure S5 in Supporting Information S1).

### 3.3. Float Analysis

Given the sparsity of historical measurements in the Southern Ocean, remote sensing is an invaluable tool to study the region. However, satellite algorithms have been shown to underestimate SChl in the Southern Ocean



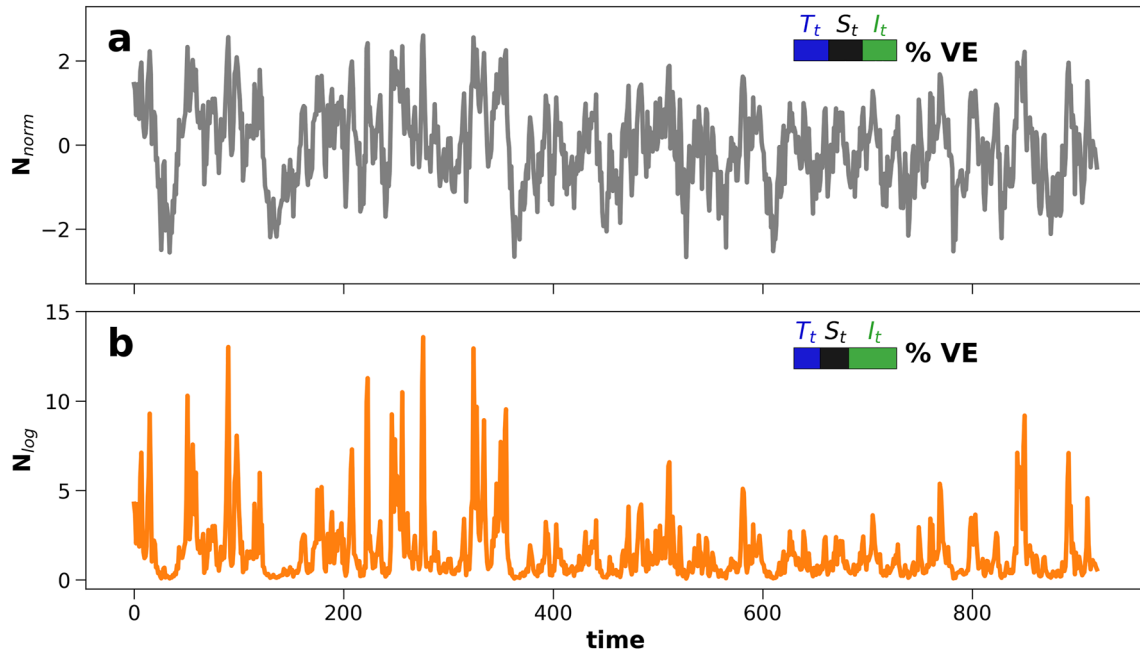


**Figure 5.** Synthetic timeseries of red noise generated by an auto-regressive process with (a) zero-mean and Gaussian distribution and (b) positive-valued and log-normal distribution. In both panels, insets show the percent variance explained by low (blue), mid (black), and high (green) frequency bands. These values are  $T_t = 33\%$ ,  $S_t = 32\%$ ,  $I_t = 34\%$  in (a), and  $T_t = 27\%$ ,  $S_t = 26\%$ ,  $I_t = 46\%$  in (b).

compared to in situ measurements (Kahru & Mitchell, 2010). Furthermore, changes in SChl do not necessarily reflect changes in the integrated biomass (Carranza et al., 2018; Uchida et al., 2019). It is possible, for example, that sub-seasonal SChl variability is simply due to dilution of the surface signal by episodic mixing, rather than high-frequency changes in phytoplankton biomass. To assess this, we analyze subsurface data from three autonomous floats deployed near Kerguelen Plateau by the SOCLIM project (Pellichero et al., 2020). Figure 6 shows the vertical chlorophyll section from float 6902735, as well as the comparison of SChl and  $\text{Chl}_{\text{tot}}$  timeseries.

While much of the chlorophyll signal is subsurface, the SChl and  $\text{Chl}_{\text{tot}}$  timeseries are reasonably well correlated ( $R = 0.81$ ), albeit less so at sub-seasonal timescales ( $R = 0.66$ ). This was found by applying the same decomposition method outlined in Section 2.2 to float SChl and  $\text{Chl}_{\text{tot}}$  (Figure 7). For SChl, the percentages of variance explained by the multi-annual, seasonal, and sub-seasonal components are 9%, 46%, and 44%, respectively, while for  $\text{Chl}_{\text{tot}}$ , the percentages of variance explained by the multi-annual, seasonal, and sub-seasonal components are 8%, 55%, and 36%, respectively. In other words, sub-seasonal variability is stronger for SChl compared to  $\text{Chl}_{\text{tot}}$ , which implies larger variations in biological rates and concentrations near the surface than at depth. This could be, in part, due to dilution of the surface signal rather than changes in total biomass. Although, sub-seasonal  $\text{Chl}_{\text{tot}}$  variability still contributes a large share to the total variance and exceeds the multi-annual component, as we see for SChl. The same conclusion was drawn from the other two SOCLIM floats analyzed (floats IDs: 6902736 and 6902737); analogous plots are shown in the Supporting Information (Figures S6-S9 in Supporting Information S1). This suggests that the results based on satellite SChl data (Section 3.1) are relevant to the vertically integrated chlorophyll, although possibly slightly overestimating the contribution of sub-seasonal timescales to the total variability.

#### 4. Discussion and Conclusions

Satellite data and autonomous float measurements analyzed here show that sub-seasonal SChl variability exceeds multi-annual variability in the Southern Ocean. As a result, year-to-year variations of annual mean SChl primarily reflect high-frequency events rather than low-frequency variability (Little et al., 2018). This is because, within the ACC, the annual mean SChl value itself results from the sum of intermittent pulses occurring at weekly timescales (or at shorter timescales not resolved by the satellite data set). Therefore, the annual mean SChl is higher in years with more or larger pulses, which is confirmed by high correlations between annual mean SChl and annual

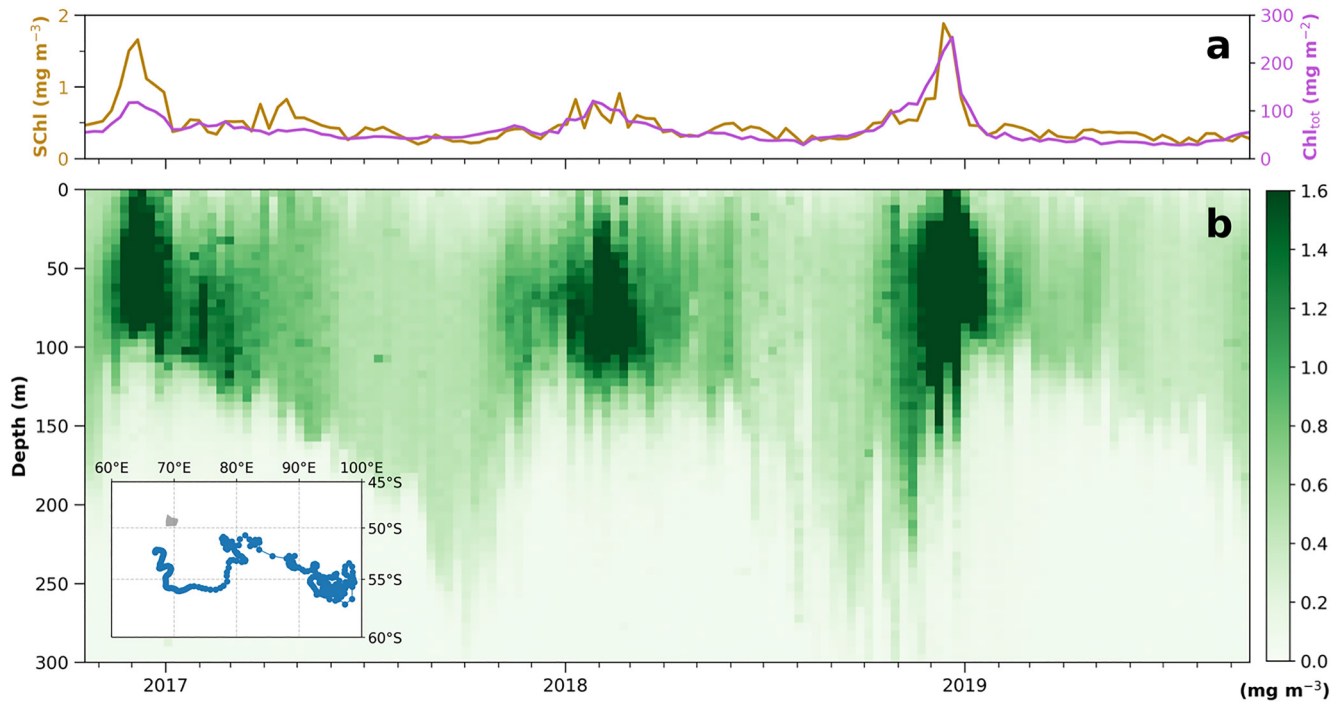


**Figure 6.** Float 6902735 (a) satellite-derived surface chlorophyll (gold) and  $Chl_{tot}$  (purple) timeseries, as well as (b) vertical chlorophyll section with inlay showing float trajectory.

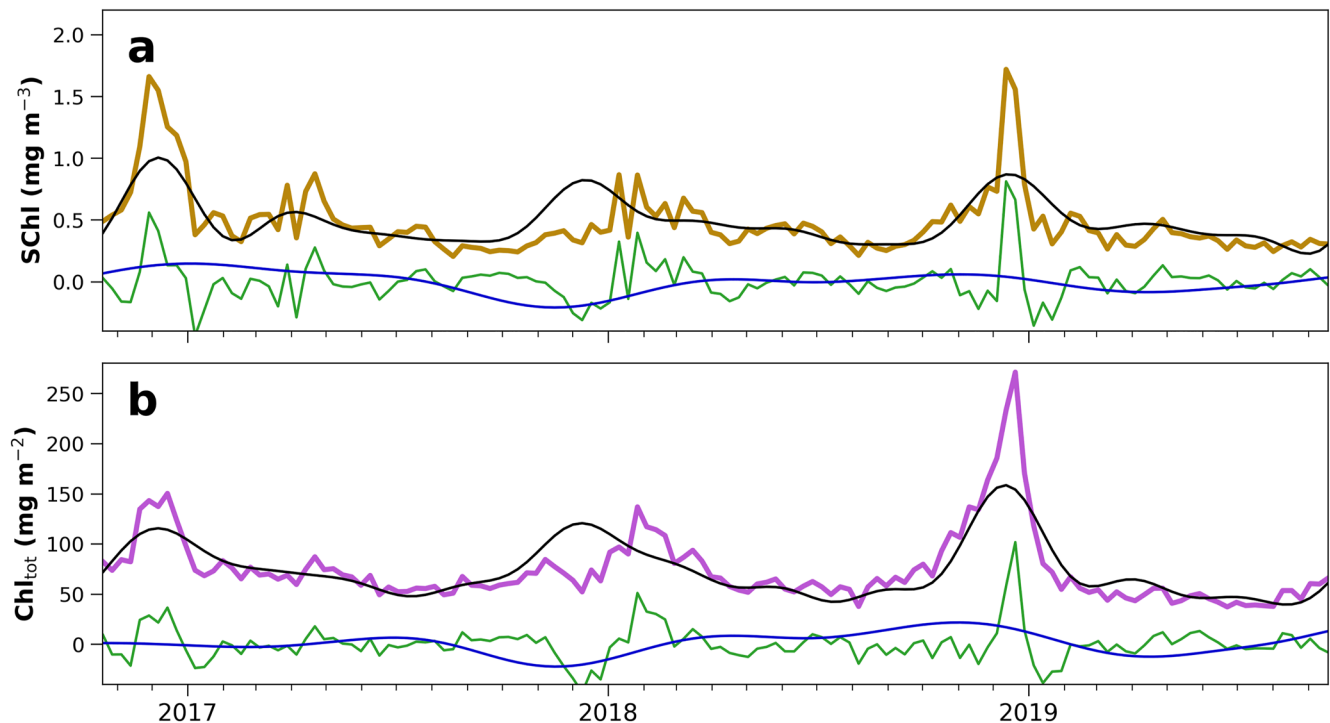


**Figure 7.** Timeseries decomposition of float 6902735 (a) Satellite-derived surface chlorophyll, full signal in gold, and (b)  $Chl_{tot}$ , full signal in purple. In both panels the multi-annual component is blue, the seasonal component is black, and the sub-seasonal component is green.

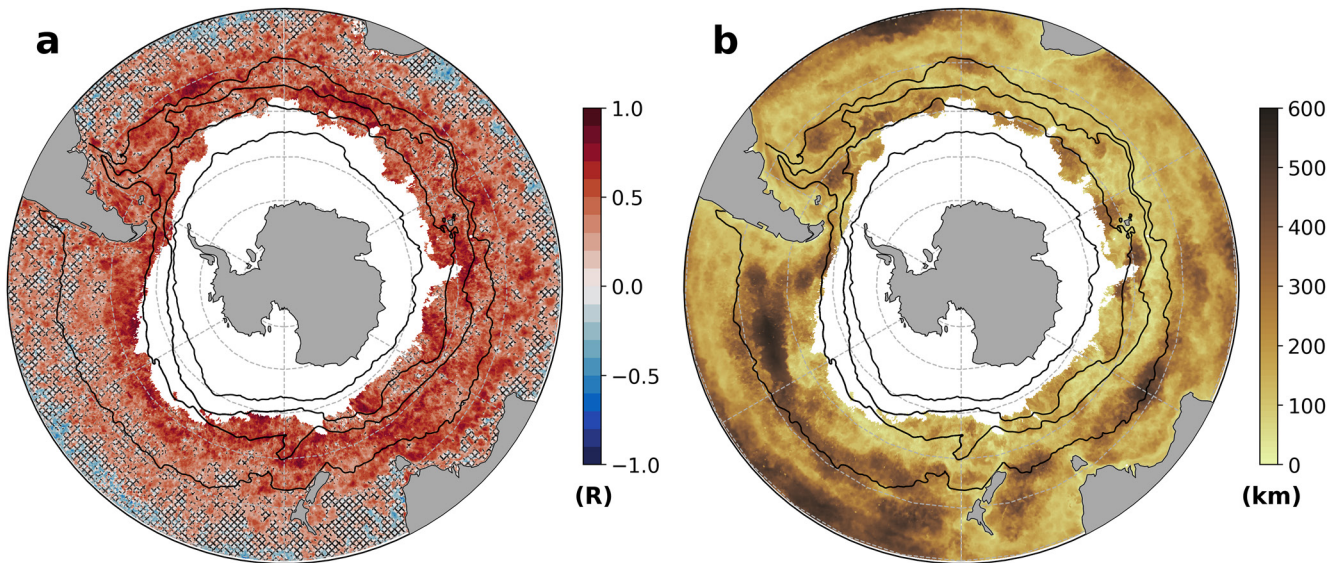


**Figure 8.** (a) Correlation coefficient between annual mean satellite-derived surface chlorophyll (SChl) and annual variance in the sub-seasonal component of SChl. Cross-hatching indicates where the correlations are not significant at the 95% level. (b) Length scale (km) associated with consistent variations in annual mean SChl.

variance of the sub-seasonal component of SChl (Figure 8a). The inverse cascade toward low frequencies could result from ecological fluctuations or from changes in the prevalence of extreme wind events or eddy activity (Cravatte et al., 2021), which in turn may be connected to climate variability (Busecke & Abernathy, 2019; Hell et al., 2021), although sub-seasonal SChl variations were only weakly correlated with the SAM index (Figure 4d).

The link between annual mean SChl and high-frequency events is important because sub-seasonal SChl variability occurs at spatial scales of ~50–150 km (Figure S1c in Supporting Information S1), which leads to a similarly small spatial autocorrelation for variations in annual mean SChl (Figure 8b). In the ACC, the average length scale associated with correlated fluctuations in annual mean SChl is only 260 km. This is in contrast to the seasonal cycle of SChl, which is forced, to leading order, by large-scale changes in solar irradiance and surface stratification, and thus has much larger spatial scales, ~600 km (Figure S1b in Supporting Information S1). For example, vast bloom phenology regimes have been defined based on SChl seasonality, and approximately correspond to the frontal zones of the ACC (Ardyna et al., 2017; Sallée et al., 2015; Thomalla et al., 2011). Indeed, averaging the satellite data over the Subtropical Zone (STZ), Subantarctic Zone (SAZ), and the ACC—as defined by the mean frontal positions from Kim and Orsi (2014), see Supporting Information—shows that, in a given frontal zone, the seasonal component of SChl ( $S$ ) has a small standard error (Figure 9a); this means that the seasonal cycle is relatively consistent across all grid cells, although note that the calculation of standard error assumes Gaussian statistics. However, the full SChl signal ( $X$ ) has larger standard errors within a frontal zone (Figure 9b), particularly in the SAZ and ACC where sub-seasonal variability is strong. This is also reflected in the fluctuations of annual mean SChl, which have large standard errors in the SAZ and in the ACC (Figure 9c), despite the regularity of the seasonal cycle over these zones. In other words, the bioregions defined based on phytoplankton seasonality or time-mean SChl are not necessarily meaningful in the context of year-to-year variations.

These results suggest that changes in annual mean SChl are tied to the forcing that drives sub-seasonal SChl fluctuations. This includes anomalies in wind stress or surface buoyancy forcing (Carranza & Gille, 2015; Keerthi et al., 2021; Swart et al., 2015), oceanic mesoscale and sub-mesoscale variability (Frenger et al., 2018; McGillicuddy, 2016; Whitt, Lévy, & Taylor, 2019), or ecosystem interactions such as top-down controls from grazing (Arteaga et al., 2020; Behrenfeld & Boss, 2014), competition for multiple resources (Huisman & Weissing, 2001), and interactions between the two (Mayersohn et al., 2021). It is difficult to separate the effects of these mechanisms for several reasons. First, the timescales associated with mesoscale and submesoscale physical processes overlap with those of intrinsic ecosystem variability. Second, the sign of the SChl response to wind or MLD perturbations exhibits significant seasonal and regional variability (Le Quéré et al., 2002; Llort et al., 2019). For example, several studies have observed a seasonal progression from light limitation to nutrient limitation in the Southern Ocean (Li et al., 2021; Ryan-Keogh et al., 2018; von Berg et al., 2020). In a light-limited regime,

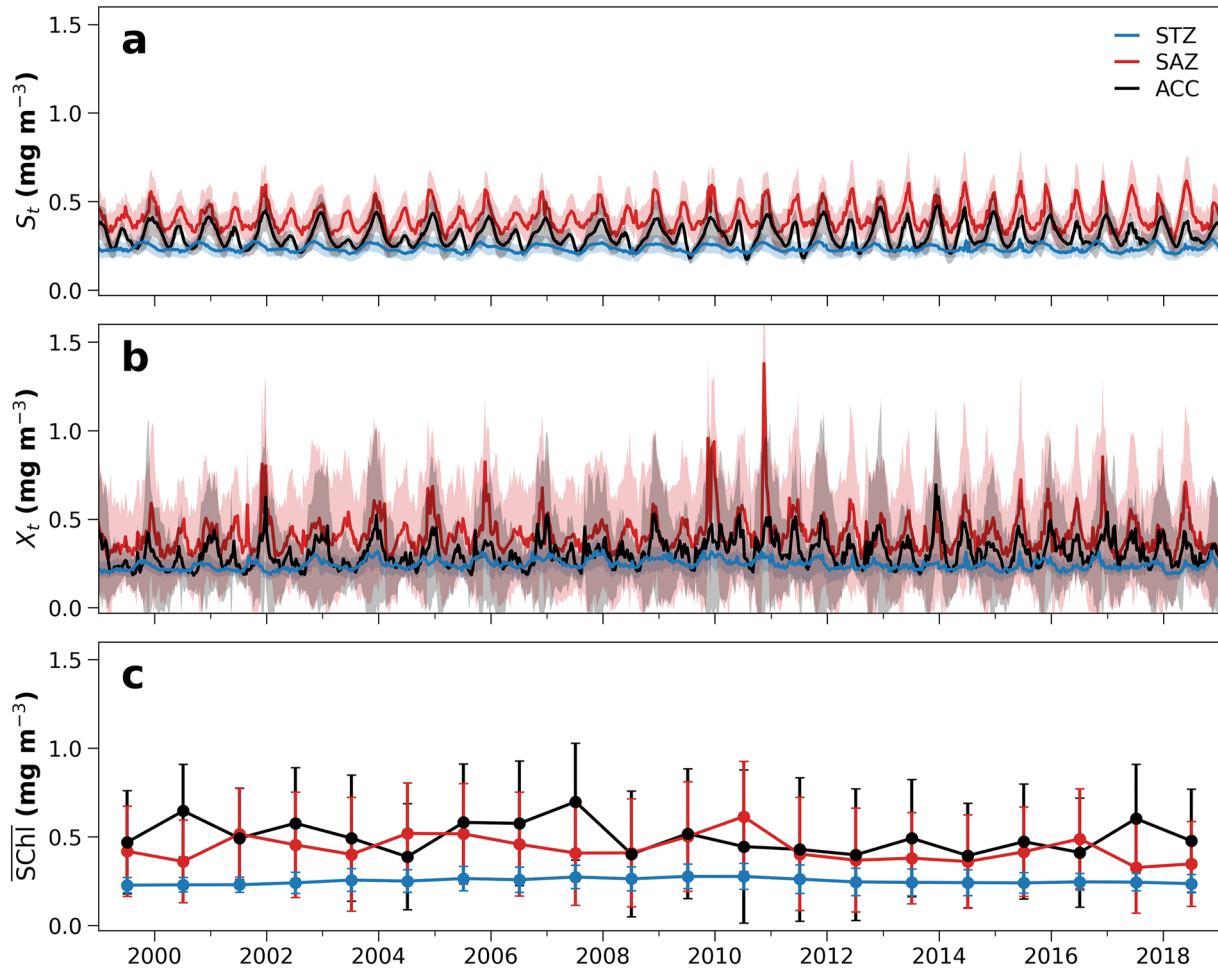


**Figure 9.** (a) Seasonal component of satellite-derived surface chlorophyll (SChl) ( $S_t$ ) averaged over the Subtropical Zone, Subantarctic Zone, and Antarctic Circumpolar Current, as defined by the Kim and Orsi (2014) fronts. (b) Full SChl signal ( $X_t$ ) averaged over the same frontal zones as in (a). (c) Annual mean SChl ( $\overline{\text{SChl}}$ ) for each frontal zone plotted at the mid-point of each respective year (i.e., 2nd July). Error bars reflect the standard error of all grid cells within each frontal zone.

phytoplankton growth is associated with restratification due to decreased winds and/or submesoscale buoyancy fluxes (du Plessis et al., 2017; Pellichero et al., 2020; Swart et al., 2015; Thomalla et al., 2015). In contrast, in a nutrient-limited regime, increases in SChl are driven by transient nutrient entrainment from storm-driven mixing (Carranza & Gille, 2015), eddy activity (Uchida et al., 2020), or wind-eddy interactions (du Plessis et al., 2019; Gille et al., 2014).

Untangling these mechanisms has important implications for year-to-year variability. For example, if sub-seasonal SChl fluctuations are driven primarily by wind-driven nutrient entrainment from synoptic storms, then annual mean SChl could presumably be linked to storm frequency. In contrast, if sub-seasonal SChl fluctuations are forced by oceanic (sub-)mesoscale variability, then annual mean SChl would possibly be connected to changes in EKE. Finally, some studies suggest that the surface iron supply is set by wintertime mixing (Nicholson et al., 2019; Tagliabue et al., 2014), in which case annual mean SChl would potentially be related to the previous winter's maximum MLD. Testing these hypotheses is difficult using observations. We tried, for example, to correlate annual mean SChl with summer storm frequency (Figure S10 in Supporting Information S1), defined as the percentage of days in summer (DJF) with daily mean wind speed greater than 10 m/s (Carranza et al., 2018). The correlations are relatively modest, but this could be due to inaccuracy in the wind product at high frequencies, decoupling in time between mixing and wind stress at sub-seasonal timescales (Whitt et al., 2017), the nonlinear relationship between MLD and surface forcing (Whitt, Nicholson, & Carranza, 2019), or variability in the phytoplankton response to MLD perturbations (Llort et al., 2019). Other studies (e.g., Li et al., 2021) have additionally

shown a weak relationship between annual mean production and MLD. However, further work is needed to quantify the contribution of these different processes to the total year-to-year variability.

While many previous studies have examined sub-seasonal SChl variability and have highlighted the complex mechanisms at play, the role of high-frequency fluctuations in driving the annual mean SChl and its variability is not widely recognized. Non-seasonal SChl variability in the Southern Ocean has often been attributed to the SAM (Greaves et al., 2020; Lovenduski & Gruber, 2005). However, here we have shown that low-frequency SChl fluctuations, which show a relationship to the SAM index, are dwarfed by the much larger amplitude sub-seasonal variability. Therefore, year-to-year changes in annual mean SChl reflect episodic forcing, such as storms and eddies, rather than multi-annual climate variability. Although future work should investigate the role of climate modes in modulating the prevalence and magnitude of synoptic events and (sub-)mesoscale mixing (Busecke & Abernathy, 2019; Hell et al., 2021). One implication of these results is that annual mean SChl only varies consistently over small spatial scales. Consequently, developing a mechanistic understanding of year-to-year variations in Southern Ocean primary production is an inherently local question that requires resolving sub-seasonal, small-scale processes.

### Data Availability Statement

8-day composites of satellite surface chlorophyll are available from European Space Agency Ocean Color Climate Change Initiative (<http://www.oceancolour.org/>). Profiling float data were collected and made freely available by the Southern Ocean and Climate Field Studies with Innovative Tools project (<http://soclilm.com/>). Daily wind speeds from the merged Cross-Calibrated Multi Platform product are available online (<http://www.remss.com/measurements/ccmp/>). The daily Antarctic Oscillation index is available from the NOAA/NCEP Climate Prediction Center (<http://www.cpc.ncep.noaa.gov/>). Mean EKE is calculated from a NOAA surface drifter climatology ([http://www.aoml.noaa.gov/phod/gdp/mean\\_velocity.php](http://www.aoml.noaa.gov/phod/gdp/mean_velocity.php)).

### Acknowledgments

CJP, STG, and LDT are supported by NSF OPP-1936222. CJP was also supported by a National Science Foundation Graduate Research Fellowship under Grant DGE-1650112 and a Chateaubriand Fellowship from the Office for Science and Technology of the Embassy of France in the United States. MGK is supported by a postdoctoral fellowship from CNRS. ML and OA acknowledge support from ANR-SOBUMS under contract number ANR-16-CE01-0014.

### References

- Allen, M. R., & Smith, L. A. (1996). Monte Carlo SSA: Detecting irregular oscillations in the presence of colored noise. *Journal of Climate*, 9(12), 3373–3404. [https://doi.org/10.1175/1520-0442\(1996\)009<3373:mcsdio>2.0.co;2](https://doi.org/10.1175/1520-0442(1996)009<3373:mcsdio>2.0.co;2)
- Ardyna, M., Claustre, H., Sallée, J.-B., D'Ovidio, F., Gentili, B., van Dijken, G., et al. (2017). Delineating environmental control of phytoplankton biomass and phenology in the Southern Ocean. *Geophysical Research Letters*, 44(10), 5016–5024. <https://doi.org/10.1002/2016gl072428>
- Arrigo, K. R., van Dijken, G. L., & Bushinsky, S. (2008). Primary production in the Southern Ocean, 1997–2006. *Journal of Geophysical Research*, 113(C8), C08004. <https://doi.org/10.1029/2007jc004551>
- Arteaga, L. A., Boss, E., Behrenfeld, M. J., Westberry, T. K., & Sarmiento, J. L. (2020). Seasonal modulation of phytoplankton biomass in the Southern Ocean. *Nature Communications*, 11(1), 5364. <https://doi.org/10.1038/s41467-020-19157-2>
- Atlas, R., Hoffman, R. N., Ardizzone, J., Leidner, S. M., Jusem, J. C., Smith, D. K., & Gombos, D. (2011). A cross-calibrated, multiplatform ocean surface wind velocity product for meteorological and oceanographic applications. *Bulletin of the American Meteorological Society*, 92(2), 157–174. <https://doi.org/10.1175/2010bams2946.1>
- Behrenfeld, M. J., & Boss, E. S. (2014). Resurrecting the ecological underpinnings of ocean plankton blooms. *Annual Review of Marine Science*, 6(1), 167–194. <https://doi.org/10.1146/annurev-marine-052913-021325>
- Behrenfeld, M. J., O'Malley, R. T., Siegel, D. A., McClain, C. R., Sarmiento, J. L., Feldman, G. C., et al. (2006). Climate-driven trends in contemporary ocean productivity. *Nature*, 444(7120), 752–755. <https://doi.org/10.1038/nature05317>
- Bonhomme, C., Aumont, O., & Echevin, V. (2007). Advective transport caused by intraseasonal rossby waves: A key player of the high chlorophyll variability off the Peru upwelling region. *Journal of Geophysical Research*, 112(C9), C09018. <https://doi.org/10.1029/2006jc004022>
- Boyd, P. W., Doney, S. C., Strzepek, R., Dusenberry, J., Lindsay, K., & Fung, I. (2008). Climate-mediated changes to mixed-layer properties in the Southern Ocean: Assessing the phytoplankton response. *Biogeosciences*, 5(3), 847–864. <https://doi.org/10.5194/bg-5-847-2008>
- Busecke, J. J. M., & Abernathy, R. P. (2019). Ocean mesoscale mixing linked to climate variability. *Science Advances*, 5(1), eaav5014. <https://doi.org/10.1126/sciadv.aav5014>
- Campbell, J. W. (1995). The lognormal distribution as a model for bio-optical variability in the sea. *Journal of Geophysical Research*, 100(C7), 13237–13254. <https://doi.org/10.1029/95jc00458>
- Carranza, M. M., & Gille, S. T. (2015). Southern Ocean wind-driven entrainment enhances satellite chlorophyll-a through the summer. *Journal of Geophysical Research: Oceans*, 120(1), 304–323. <https://doi.org/10.1002/2014jc010203>
- Carranza, M. M., Gille, S. T., Franks, P. J. S., Johnson, K. S., Pinkel, R., & Girtton, J. B. (2018). When mixed layers are not mixed. Storm-driven mixing and bio-optical vertical gradients in mixed layers of the Southern Ocean. *Journal of Geophysical Research: Oceans*, 123(10), 7264–7289. <https://doi.org/10.1029/2018jc014416>
- Cravatte, S., Serazin, G., Penduff, T., & Menkes, C. (2021). Imprint of chaotic ocean variability on transports in the southwestern Pacific at interannual timescales. *Ocean Science*, 17(2), 487–507. <https://doi.org/10.5194/os-17-487-2021>
- de Baar, H. J. W., de Jong, J. T. M., Bakker, D. C. E., Löscher, B. M., Veth, C., Bathmann, U., & Smetacek, V. (1995). Importance of iron for plankton blooms and carbon dioxide drawdown in the Southern Ocean. *Nature*, 373(6513), 412–415. <https://doi.org/10.1038/373412a0>
- du Plessis, M., Swart, S., Anson, I. J., & Mahadevan, A. (2017). Submesoscale processes promote seasonal restratification in the Subantarctic Ocean. *Journal of Geophysical Research: Oceans*, 122(4), 2960–2975. <https://doi.org/10.1002/2016jc012494>

- du Plessis, M., Swart, S., Anson, I. J., Mahadevan, A., & Thompson, A. F. (2019). Southern Ocean seasonal restratification delayed by submesoscale wind-front interactions. *Journal of Physical Oceanography*, 49(4), 1035–1053. <https://doi.org/10.1175/jpo-d-18-0136.1>
- Fauchereau, N., Tagliabue, A., Bopp, L., & Monteiro, P. M. (2011). The response of phytoplankton biomass to transient mixing events in the Southern Ocean. *Geophysical Research Letters*, 38(17), L17601. <https://doi.org/10.1029/2011gl048498>
- Frenger, I., Münnich, M., & Gruber, N. (2018). Imprint of Southern Ocean mesoscale eddies on chlorophyll. *Biogeosciences*, 15, 4781–4798. <https://doi.org/10.5194/bg-15-4781-2018>
- Gille, S. T., Carranza, M. M., Cambra, R., & Morrow, R. (2014). Wind-induced upwelling in the Kerguelen Plateau region. *Biogeosciences*, 11(22), 6389–6400. <https://doi.org/10.5194/bg-11-6389-2014>
- Graham, R. M., De Boer, A. M., van Sebille, E., Kohfeld, K. E., & Schlosser, C. (2015). Inferring source regions and supply mechanisms of iron in the Southern Ocean from satellite chlorophyll data. *Deep Sea Research Part I: Oceanographic Research Papers*, 104, 9–25. <https://doi.org/10.1016/j.dsr.2015.05.007>
- Greaves, B. L., Davidson, A. T., Fraser, A. D., McKinlay, J. P., Martin, A., McMinn, A., & Wright, S. W. (2020). The Southern Annular Mode (SAM) influences phytoplankton communities in the seasonal ice zone of the Southern Ocean. *Biogeosciences*, 17(14), 3815–3835. <https://doi.org/10.5194/bg-17-3815-2020>
- Gregg, W. W., & Rousseaux, C. S. (2019). Global ocean primary production trends in the modern ocean color satellite record (1998–2015). *Environmental Research Letters*, 14(12), 124011. <https://doi.org/10.1088/1748-9326/ab4667>
- Grenier, M., Della Penna, A., & Trull, T. W. (2015). Autonomous profiling float observations of the high-biomass plume downstream of the Kerguelen Plateau in the Southern Ocean. *Biogeosciences*, 12(9), 2707–2735. <https://doi.org/10.5194/bg-12-2707-2015>
- Haëntjens, N., Boss, E., & Talley, L. D. (2017). Revisiting Ocean Color algorithms for chlorophyll a and particulate organic carbon in the Southern Ocean using biogeochemical floats. *Journal of Geophysical Research: Oceans*, 122(8), 6583–6593. <https://doi.org/10.1002/2017jc012844>
- Hanawa, K., & Talley, L. D. (2001). Mode waters. In G. Siedler, J. Church, & J. Gould (Eds.), *ocean circulation and climate* (Vol. 77, pp. 373–386). Academic Press.
- Hell, M., Cornuelle, B. D., Gille, S. T., & Lutsko, N. J. (2021). Time-varying empirical probability densities of Southern Ocean surface winds: Linking the leading mode to SAM and quantifying wind product differences. *Journal of Climate*, 34, 5497–5522. <https://doi.org/10.1175/jcli-d-20-0629.1>
- Henson, S. A., Sarmiento, J. L., Dunne, J. P., Bopp, L., Lima, I., Doney, S. C., et al. (2010). Detection of anthropogenic climate change in satellite records of ocean chlorophyll and productivity. *Biogeosciences*, 7(2), 621–640. <https://doi.org/10.5194/bg-7-621-2010>
- Huisman, J., & Weissing, F. J. (2001). Biological conditions for oscillations and chaos generated by multispecies competition. *Ecology*, 82(10), 2682–2695. [https://doi.org/10.1890/0012-9658\(2001\)082\[2682:bcofac\]2.0.co;2](https://doi.org/10.1890/0012-9658(2001)082[2682:bcofac]2.0.co;2)
- Johnson, K. S., Plant, J. N., Coletti, L. J., Jannasch, H. W., Sakamoto, C. M., Riser, S. C., et al. (2017). Biogeochemical sensor performance in the SOCCOM profiling float array. *Journal of Geophysical Research: Oceans*, 122(8), 6416–6436. <https://doi.org/10.1002/2017jc012838>
- Joubert, W. R., Swart, S., Tagliabue, A., Thomalla, S. J., & Monteiro, P. M. S. (2014). The sensitivity of primary productivity to intra-seasonal mixed layer variability in the sub-Antarctic Zone of the Atlantic Ocean. *Biogeosciences Discussions*, 11, 4335–4358.
- Kahru, M., & Mitchell, B. G. (2010). Blending of ocean colour algorithms applied to the Southern Ocean. *Remote Sensing Letters*, 1(2), 119–124. <https://doi.org/10.1080/01431160903547940>
- Keerthi, M. G., Lévy, M., & Aumont, O. (2021). Intermittency in phytoplankton bloom triggered by modulations in vertical stability. *Scientific Reports*, 11(1), 1285. <https://doi.org/10.1038/s41598-020-80331-z>
- Keerthi, M. G., Lévy, M., Aumont, O., Lengaigne, M., & Antoine, D. (2020). Contrasted contribution of intraseasonal time scales to surface chlorophyll variations in a bloom and an oligotrophic regime. *Journal of Geophysical Research: Oceans*, 125(5), e2019JC015701. <https://doi.org/10.1029/2019jc015701>
- Keppeler, L., & Landschützer, P. (2019). Regional wind variability modulates the Southern Ocean carbon sink. *Scientific Reports*, 9(1), 7384. <https://doi.org/10.1038/s41598-019-43826-y>
- Kim, Y. S., & Orsi, A. H. (2014). On the variability of Antarctic Circumpolar Current fronts inferred from 1992–2011 altimetry. *Journal of Physical Oceanography*, 44(12), 3054–3071. <https://doi.org/10.1175/jpo-d-13-0217.1>
- Lancelot, C., de Montety, A., Goosse, H., Becquevort, S., Schoemann, V., Pasquer, B., & Vancoppenolle, M. (2009). Spatial distribution of the iron supply to phytoplankton in the Southern Ocean: A model study. *Biogeosciences*, 6(12), 2861–2878. <https://doi.org/10.5194/bg-6-2861-2009>
- Laurindo, L., Mariano, A., & Lumpkin, R. (2017). An improved near-surface velocity climatology for the global ocean from drifter observations. *Deep-Sea Research I*, 124, 73–92. <https://doi.org/10.1016/j.dsr.2017.04.009>
- Le Quéré, C., Bopp, L., & Tegen, I. (2002). Antarctic circumpolar wave impact on marine biology: A natural laboratory for climate change study. *Geophysical Research Letters*, 29(10), 45–45. <https://doi.org/10.1029/2001gl014585>
- Lévy, M., Ferrari, R., Franks, P. J. S., Martin, A. P., & Rivière, P. (2012). Bringing physics to life at the submesoscale. *Geophysical Research Letters*, 39(14), L14602. <https://doi.org/10.1029/2012gl052756>
- Lévy, M., Resplandy, L., & Lengaigne, M. (2014). Oceanic mesoscale turbulence drives large biogeochemical interannual variability at middle and high latitudes. *Geophysical Research Letters*, 41(7), 2467–2474. <https://doi.org/10.1002/2014gl059608>
- Li, Z., Lozier, M. S., & Cassar, N. (2021). Linking Southern Ocean mixed-layer dynamics to net community production on various timescales. *Journal of Geophysical Research: Oceans*, 126(10), e2021JC017537. <https://doi.org/10.1029/2021jc017537>
- Little, H. J., Vichi, M., Thomalla, S. J., & Swart, S. (2018). Spatial and temporal scales of chlorophyll variability using high-resolution glider data. *Journal of Marine Systems*, 187, 1–12. <https://doi.org/10.1016/j.jmarsys.2018.06.011>
- Llort, J., Lévy, M., Sallée, J.-B., & Tagliabue, A. (2019). Nonmonotonic response of primary production and export to changes in mixed-layer depth in the Southern Ocean. *Geophysical Research Letters*, 46(6), 3368–3377. <https://doi.org/10.1029/2018gl081788>
- Lovenduski, N. S., & Gruber, N. (2005). Impact of the southern annular mode on Southern Ocean circulation and biology. *Geophysical Research Letters*, 32(11), L11603. <https://doi.org/10.1029/2005gl022727>
- Maraun, D., Kurths, J., & Holschneider, M. (2007). Nonstationary Gaussian processes in wavelet domain: Synthesis, estimation, and significance testing. *Physical Review E*, 75(1), 016707. <https://doi.org/10.1103/physreve.75.016707>
- Martinez, E., Antoine, D., D’Ortenzio, F., & Gentili, B. (2009). Climate-driven basin-scale decadal oscillations of oceanic phytoplankton. *Science*, 326(5957), 1253–1256. <https://doi.org/10.1126/science.1177012>
- Mayersohn, B., Smith, S. K., Mangolte, I., & Lévy, M. (2021). Intrinsic timescales of variability in a marine plankton model. *Ecological Modelling*, 443, 109446. <https://doi.org/10.1016/j.ecolmodel.2021.109446>
- McGillcuddy, D. J. (2016). Mechanisms of physical-biological-biogeochemical interaction at the oceanic mesoscale. *Annual Review of Marine Science*, 8(1), 125–159. <https://doi.org/10.1146/annurev-marine-010814-015606>
- Meijers, A. J. S., Cerovečki, I., King, B. A., & Tamsitt, V. (2019). A see-saw in Pacific Subantarctic Mode Water formation driven by atmospheric modes. *Geophysical Research Letters*, 46(22), 13152–13160. <https://doi.org/10.1029/2019gl085280>

- Meredith, M. P., Watkins, J. L., Murphy, E. J., Cunningham, N. J., Wood, A. G., Korb, R., et al. (2003). An anticyclonic circulation above the northwest Georgia rise, Southern Ocean. *Geophysical Research Letters*, *30*(20), 2061. <https://doi.org/10.1029/2003gl018039>
- Mitchell, B. G., Brody, E. A., Holm-Hansen, O., McClain, C., & Bishop, J. (1991). Light limitation of phytoplankton biomass and macronutrient utilization in the Southern Ocean. *Limnology & Oceanography*, *36*(8), 1662–1677. <https://doi.org/10.4319/lo.1991.36.8.1662>
- Morel, A. (1988). Optical modeling of the upper ocean in relation to its biogenous matter content (Case I waters). *Journal of Geophysical Research*, *93*(C9), 10749–10768. <https://doi.org/10.1029/jc093ic09p10749>
- Nicholson, S.-A., Lévy, M., Jouanno, J., Capet, X., Swart, S., & Monteiro, P. M. S. (2019). Iron supply pathways between the surface and subsurface waters of the Southern Ocean: From winter entrainment to summer storms. *Geophysical Research Letters*, *46*(24), 14567–14575. <https://doi.org/10.1029/2019gl084657>
- Pellichero, V., Boutin, J., Claustre, H., Merlivat, L., Salée, J.-B., & Blain, S. (2020). Relaxation of wind stress drives the abrupt onset of biological carbon uptake in the kerguelen bloom: A multisensor approach. *Geophysical Research Letters*, *47*(9), e2019GL085992. <https://doi.org/10.1029/2019gl085992>
- Prend, C. J., Gille, S. T., Talley, L. D., Mitchell, B. G., Rosso, I., & Mazloff, M. R. (2019). Physical drivers of phytoplankton bloom initiation in the Southern Ocean's Scotia Sea. *Journal of Geophysical Research: Oceans*, *124*(8), 5811–5826. <https://doi.org/10.1029/2019jc015162>
- Resplandy, L., Vialard, J., Lévy, M., Aumont, O., & Dandonneau, Y. (2009). Seasonal and intraseasonal biogeochemical variability in the thermocline ridge of the southern tropical Indian Ocean. *Journal of Geophysical Research*, *114*(C7), C07024. <https://doi.org/10.1029/2008jc005246>
- Rintoul, S. R. (2018). The global influence of localized dynamics in the Southern Ocean. *Nature*, *558*(7709), 209–218. <https://doi.org/10.1038/s41586-018-0182-3>
- Rohr, T., Long, M. C., Kavanaugh, M. T., Lindsay, K., & Doney, S. C. (2017). Variability in the mechanisms controlling Southern Ocean phytoplankton bloom phenology in an ocean model and satellite observations. *Global Biogeochemical Cycles*, *31*(5), 922–940. <https://doi.org/10.1002/2016gb005615>
- Rosso, I., Hogg, A. M., Matear, R., & Strutton, P. G. (2016). Quantifying the influence of sub-mesoscale dynamics on the supply of iron to Southern Ocean phytoplankton blooms. *Deep Sea Research Part I: Oceanographic Research Papers*, *115*, 199–209. <https://doi.org/10.1016/j.dsr.2016.06.009>
- Rousseaux, C. S., & Gregg, W. W. (2014). Interannual variation in phytoplankton primary production at a global scale. *Remote Sensing*, *9*, 1–19. <https://doi.org/10.3390/rs6010001>
- Ryan-Keogh, T. J., Thomalla, S. J., Mtshali, T. N., van Horsten, N. R., & Little, H. J. (2018). Seasonal development of iron limitation in the sub-Antarctic zone. *Biogeosciences*, *15*(14), 4647–4660. <https://doi.org/10.5194/bg-15-4647-2018>
- Sallée, J.-B., Llorc, J., Tagliabue, A., & Lévy, M. (2015). Characterization of distinct bloom phenology regimes in the Southern Ocean. *ICES Journal of Marine Science*, *72*(6), 1985–1998. <https://doi.org/10.1093/icesjms/fsv069>
- Sallée, J.-B., Speer, K. G., & Rintoul, S. R. (2010). Zonally asymmetric response of the Southern Ocean mixed-layer depth to the southern annular mode. *Nature Geoscience*, *3*(4), 273–279. <https://doi.org/10.1038/ngeo0812>
- Sathyendranath, S., Brewin, R. J. W., Jackson, T., Mélin, F., & Platt, T. (2017). Ocean-colour products for climate-change studies: What are their ideal characteristics? *Remote Sensing of Environment*, *203*, 125–138. <https://doi.org/10.1016/j.rse.2017.04.017>
- Schulte, J. A., Duffy, C., & Najjar, R. G. (2015). Geometric and topologic approaches to significance testing in wavelet analysis. *Nonlinear Processes in Geophysics*, *22*(2), 139–156. <https://doi.org/10.5194/npg-22-139-2015>
- Sokolov, S., & Rintoul, S. R. (2007). On the relationship between fronts of the Antarctic Circumpolar Current and surface chlorophyll concentrations in the Southern Ocean. *Journal of Geophysical Research*, *112*(C7), C07030. <https://doi.org/10.1029/2006jc004072>
- Swart, S., Thomalla, S. J., & Monteiro, P. M. S. (2015). The seasonal cycle of mixed layer dynamics and phytoplankton biomass in the sub-Antarctic zone: A high-resolution glider experiment. *Journal of Marine Systems*, *147*, 103–115. <https://doi.org/10.1016/j.jmarsys.2014.06.002>
- Tagliabue, A., Mtshali, T., Aumont, O., Bowie, A. R., Klunder, M. B., Roychoudhury, A. N., & Swart, S. (2012). A global compilation of dissolved iron measurements: Focus on distributions and processes in the Southern Ocean. *Biogeosciences*, *9*(6), 2333–2349. <https://doi.org/10.5194/bg-9-2333-2012>
- Tagliabue, A., Sallée, J.-B., Bowie, A. R., Lévy, M., Swart, S., & Boyd, P. W. (2014). Surface-water iron supplies in the Southern Ocean sustained by deep winter mixing. *Nature Geoscience*, *7*(4), 314–320. <https://doi.org/10.1038/ngeo2101>
- Talley, L. D., Rosso, I., Kamenkovich, I., Mazloff, M. R., Wang, J., Boss, E., et al. (2019). Southern Ocean biogeochemical float deployment strategy, with example from the Greenwich Meridian line (GO-SHIP A12). *Journal of Geophysical Research: Oceans*, *124*(1), 403–431. <https://doi.org/10.1029/2018jc014059>
- Tamsitt, V., Talley, L. D., Mazloff, M. R., & Cerovečki, I. (2015). Zonal variations in the Southern Ocean heat budget. *Journal of Climate*, *29*(18), 6563–6579. <https://doi.org/10.1175/jcli-d-15-0630.1>
- Thomalla, S. J., Fauchereau, N., Swart, S., & Monteiro, P. M. S. (2011). Regional scale characteristics of the seasonal cycle of chlorophyll in the Southern Ocean. *Biogeosciences*, *7*(10), 2849–2866. <https://doi.org/10.5194/bg-7-2849-2011>
- Thomalla, S. J., Racault, M.-F., Swart, S., & Monteiro, P. M. S. (2015). High-resolution view of the spring bloom initiation and net community production in the Subantarctic Southern Ocean using glider data. *ICES Journal of Marine Science*, *72*(6), 1999–2020. <https://doi.org/10.1093/icesjms/fsv105>
- Thompson, D. W. J., & Wallace, J. M. (2000). Annular modes in the extratropical circulation. Part I: Month-to-month variability. *Journal of Climate*, *13*(5), 1000–1016. [https://doi.org/10.1175/1520-0442\(2000\)013<1000:amitec>2.0.co;2](https://doi.org/10.1175/1520-0442(2000)013<1000:amitec>2.0.co;2)
- Torrence, C., & Compo, G. P. (1998). A practical guide to wavelet analysis. *Bulletin of the American Meteorological Society*, *79*(1), 61–78. [https://doi.org/10.1175/1520-0477\(1998\)079<0061:apgtwa>2.0.co;2](https://doi.org/10.1175/1520-0477(1998)079<0061:apgtwa>2.0.co;2)
- Uchida, T., Balwada, D., Abernathy, R., Prend, C. J., Boss, E., & Gille, S. T. (2019). Southern Ocean phytoplankton blooms observed by biogeochemical floats. *Journal of Geophysical Research: Oceans*, *124*(11), 7328–7343. <https://doi.org/10.1029/2019jc015355>
- Uchida, T., Balwada, D., Abernathy, R. P., McKinley, G. A., Smith, S. K., & Lévy, M. (2020). Vertical eddy iron fluxes support primary production in the open Southern Ocean. *Nature Communications*, *11*(1), 1125. <https://doi.org/10.1038/s41467-020-14955-0>
- Vantrepotte, V., & Mélin, F. (2009). Temporal variability of 10-year global SeaWiFS time-series of phytoplankton chlorophyll *a* concentration. *ICES Journal of Marine Science*, *66*(7), 1547–1556. <https://doi.org/10.1093/icesjms/fsp107>
- von Berg, L., Prend, C. J., Campbell, E. C., Mazloff, M. R., Talley, L. D., & Gille, S. T. (2020). Weddell Sea phytoplankton blooms modulated by sea ice variability and polynya formation. *Geophysical Research Letters*, *47*(11), e2020GL087954. <https://doi.org/10.1029/2020gl087954>
- Whitt, D. B., Lévy, M., & Taylor, J. R. (2019). Submesoscales enhance storm-driven vertical mixing of nutrients: Insights from a biogeochemical Large Eddy Simulation. *Journal of Geophysical Research: Oceans*, *124*(11), 8140–8165. <https://doi.org/10.1029/2019jc015370>
- Whitt, D. B., Nicholson, S. A., & Carranza, M. M. (2019). Global impacts of subseasonal (<60 day) wind variability on ocean surface stress, buoyancy flux, and mixed layer depth. *Journal of Geophysical Research: Oceans*, *124*(12), 8798–8831. <https://doi.org/10.1029/2019jc015166>

- Whitt, D. B., Taylor, J. R., & Lévy, M. (2017). Synoptic-to-planetary scale wind variability enhances phytoplankton biomass at ocean fronts. *Journal of Geophysical Research: Oceans*, 122(6), 4602–4633. <https://doi.org/10.1002/2016jc011899>
- Xing, X., Claustre, H., Boss, E., Roesler, C., Organelli, E., Poteau, A., et al. (2017). Correction of profiles of in-situ chlorophyll fluorometry for the contribution of fluorescence originating from non-algal matter. *Limnology and Oceanography: Methods*, 15(1), 80–93. <https://doi.org/10.1002/lom3.10144>